Applied Physics Letters

Dielectric barrier discharge control of a turbulent boundary layer in a supersonic flow

Cite as: Appl. Phys. Lett. **97**, 041503 (2010); https://doi.org/10.1063/1.3473820
Submitted: 06 April 2010 . Accepted: 12 July 2010 . Published Online: 30 July 2010

S. Im, H. Do, and M. A. Cappelli

View Online Export Citation

ARTICLES YOU MAY BE INTERESTED IN

Dielectric barrier discharge induced boundary layer suction
Applied Physics Letters **100**, 264103 (2012); https://doi.org/10.1063/1.4731288

Mach 5 bow shock control by a nanosecond pulse surface dielectric barrier discharge
Physics of Fluids **23**, 066101 (2011); https://doi.org/10.1063/1.3599697

On the role of oxygen in dielectric barrier discharge actuation of aerodynamic flows
Applied Physics Letters **91**, 181501 (2007); https://doi.org/10.1063/1.2803755

© 2010 American Institute of Physics.

Dielectric barrier discharge control of a turbulent boundary layer in a supersonic flow

S. Im,[a] H. Do, and M. A. Cappelli
Department of Mechanical Engineering, Stanford University, Stanford, California 94305-3032, USA

(Received 6 April 2010; accepted 12 July 2010; published online 30 July 2010)

We demonstrate effective manipulation of a turbulent boundary layer at Mach 4.7 conditions using a surface dielectric barrier discharge (DBD) actuator. The freestream conditions of low static pressure (1 kPa) and temperature (60 K) are conducive to the visualization of flow features using Rayleigh scattering from condensed CO_2 particles. The boundary layer thinning is observed when spanwise momentum is induced by the low power (6.8 W), low frequency (28 kHz) single actuator pair oriented parallel to the freestream flow. © *2010 American Institute of Physics*.
[doi:10.1063/1.3473820]

There have been several demonstrations in the use of surface dielectric barrier discharge (DBD) actuators for subsonic flow control[1] since their discovery by Roth *et al.*[2] A typical DBD actuator consists of an alternating-current (ac) driven exposed and surface (dielectric)-embedded electrode, designed to impose a force on ionized gas molecules generated by the discharge, and to induce a directional flow through collisions between the drifting ions with ambient neutral molecules. The discharge is asymmetric, with the force acting primarily on negative ions of oxygen[3,4] on the swing of the cycle when the embedded electrode potential is positive relative to the exposed electrode. This DBD induced directional flow, often referred to as the wall jet, can have a speed as large as about 10m/s[1] and can be effective in boundary layer separation control,[5–8] laminar-turbulent boundary layer transition delay,[9] turbulent boundary layer manipulation,[10,11] and vortex generation.[12,13]

There have been few investigations of low power DBD actuation for control of supersonic flows. Supersonic boundary layer control is currently a major issue in the development of scramjet engines. Scramjet inlet-duct boundary layer control provides an opportunity to extend engine performance and operating margin limited by unstart processes.[14] Recently, plasma-induced supersonic flow actuation was reported using very high power (~10 kW) direct-current (dc) thermal plasmas,[15] high power (100–200 W) plasma-induced wall jets,[16] and high power (100 W) streamwise-oriented dc discharges.[17] This letter presents the demonstration of turbulent boundary layer suppression in a supersonic flow by a nonthermal and low power (<10 W) DBD actuator, demonstrating the potential for such discharges as practical flow control actuators in scramjet applications.

In the present study, important flow features (e.g., boundary layers and shock waves) are visualized using Rayleigh scattering of a laser sheet from condensed CO_2 particles. Miles *et al.*[18] and Wu *et al.*[19] have proposed the use of this technique as an effective flow visualization method for low static temperature and pressure supersonic flows. Gaseous CO_2 is added to the intake stream of a supersonic wind tunnel and undergoes condensation by the sudden temperature drop during the flow expansion and acceleration. The condensed CO_2 particles sublime in regions of high static temperature such as within boundary layers. These regions are easily distinguished by the scattered laser light intensity providing high fidelity contrast in flow visualized images captured by charge coupled device (CCD) camera.

The experiment, shown schematically in Fig. 1, consists of a wind tunnel, a laser diagnostics system, and a compression ramp model with a longitudinal DBD actuator attached on its surface. The blow-down wind tunnel with a two-dimensional converging/diverging nozzle (25:1 area ratio) is used to generate the supersonic flow. The freestream Mach number is 4.7, determined by measuring the incident/reflected shock angle on a test wedge immersed into the freestream. High pressure air and CO_2 mixture (P_0 =350 kPa and T_0=300 K, 3:1 volume ratio) expands into

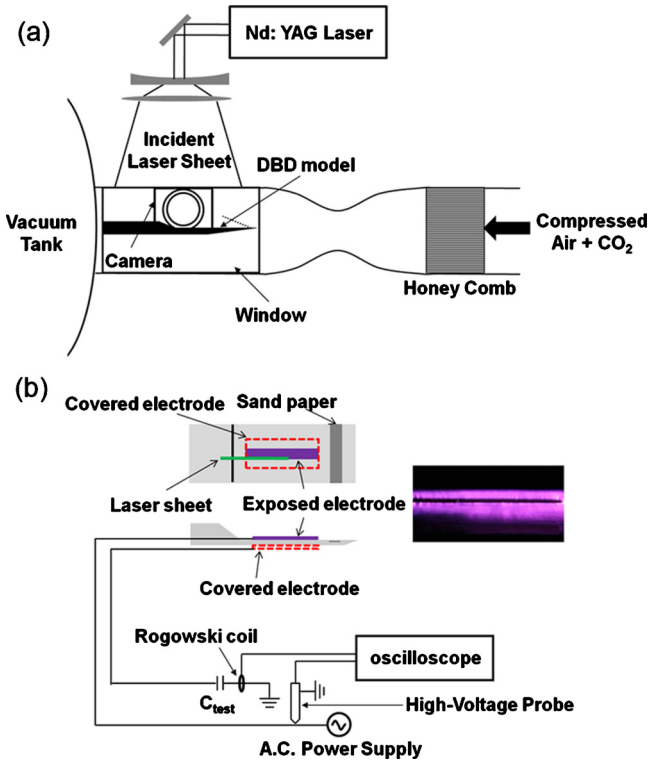

FIG. 1. (Color online) Schematic of experimental setup (a) wind tunnel with optical diagnostic system and (b) longitude DBD actuator system.

[a]Electronic mail: sim3@stanford.edu.

 © 2010 American Institute of Physics

the 40×40 mm^2 cross sectional area tunnel test section which is connected downstream to a vacuum chamber. The useful test time is approximately 5 s, limited by the pressure that can be maintained in the vacuum chamber and the static pressure and temperature of the flow in the test section during this time is approximately 1 kPa and 60 K, respectively. Optical access is provided by windows placed on both sides of test section. A Nd:YAG laser (New wave, Gemini PIV, 100mJ/pulse energy, 10Hz, 532nm) is shaped into a thin sheet using two cylindrical lenses and a convex spherical lens, and is directed into the test section. A CCD camera (La Vision, Imager Intense) detects the scattered light at 90° to the laser sheet.

A DBD actuator is integrated into the upper surface of a compression ramp model that spans the 40 mm width of the tunnel. The model has a sharp leading edge (270 mm downstream of the tunnel throat), wedged shaped on its lower surface, and a compression ramp located 120 mm downstream of this leading edge. Sand paper (180 Grit, 40 mm wide, and 20 mm long) is attached to the top of the model 10 mm downstream from the leading edge to trip the otherwise laminar boundary layer, thereby, creating a thick turbulent boundary layer easily characterized by the Rayleigh scattering diagnostic. The section of the model between the leading edge and ramp was 3 mm thick, and the portion that accommodated the DBD actuator was fabricated out of cast acrylic, with an epoxy (Loctite Hysol 1C) serving as a dielectric layer (approximately 2 mm thick) isolating the buried electrode of the DBD actuator. The DBD electrode is a single strip, oriented parallel to the flow (streamwise direction). The exposed and buried electrodes (each 0.1 mm thick) are 75 mm in length and 7 mm wide, and 85 mm in length, and 25 mm wide, respectively. The exposed electrode is centered over the buried electrode, and both electrodes are placed along the center of the model with the leading edge of the electrodes located 40 mm downstream from the model leading edge. As shown in Fig. 1(b), the laser sheet (500 μm thickness) illuminates a plane intersecting a line on the model located between 85 mm and 140 mm downstream from the leading edge and 3.5 mm off center line. An ac power supply is used to generate the surface DBD discharge. A typical image of its emission (viewed from above) while exposed to the Ma=4.7 flow taken by a digital camera with 1/30 s exposure time is presented at the upper corner of Fig. 1(b). The emission of discharge appears quite uniform under the low pressure conditions of the test section but still seems to have a filamentary structure typical of these discharges in air.

The power consumption of the DBD actuator is determined from the driving frequency and the integrated area under the characteristic charge (Q)-applied voltage (V) curve,[20,21] with the charge obtained using the time-integrated current to a 50 nF capacitor (Aerovox 1445 series) connected to the buried electrode. A Rogowski coil (Pearson Electronics, Model 2877) and a 1000:1 high voltage probe (Tektronix, P6015A) are used to record current and voltage traces, respectively. A typical voltage/current trace and Q-V curve is shown in Figs. 2(a) and 2(b), respectively, for 28 kHz, 6 kV peak to peak driving conditions. These conditions result in approximately 6.8 W of delivered power; a value much lower than what has been used in previous studies of plasma actuation of supersonic flows.[15–17]

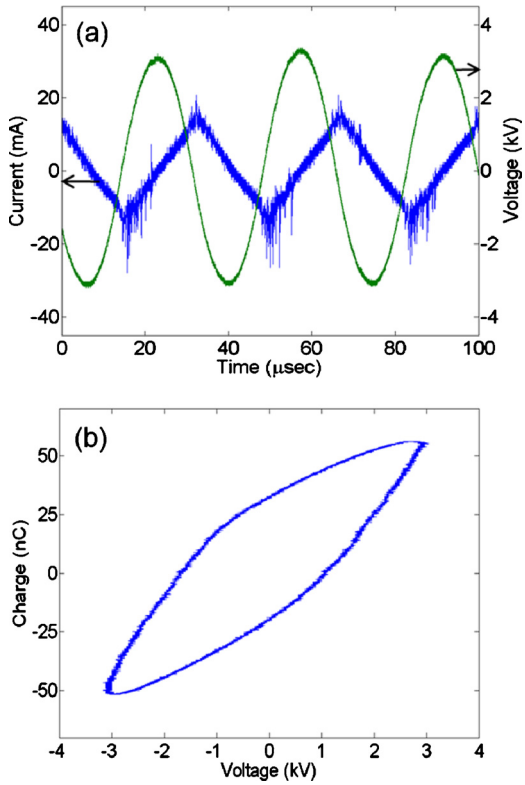

FIG. 2. (Color online) (a) Voltage and current profile of DBD and (b) characteristic Q-V curve.

Typical images obtained by CO_2 Rayleigh scattering are shown in Figs. 3(a) and 3(b) for instantaneous images, and in Figs. 3(c) and 3(d) for ten-frame averaged images for cases without and with the discharge activated, respectively. In these images, the flow is from right to left. The thickness of boundary layer can be estimated by measuring the height of dark region on the wall.[22] The boundary layer on the DBD actuator appears to be reduced significantly when the discharge is activated. In Fig. 3, the location indicated by the arrow is 25 mm upstream of the end of the DBD actuator. From a comparison of the average images at this point, we find that the boundary layer thickness with plasma forcing is less than half of that without forcing. The reduction in average boundary layer thickness is consistent with the response seen in the instantaneous images. The capability of DBD plasma actuation to reduce boundary layer thickness has potentially significant implications in that it can lead to methods of preventing or delaying the inlet unstart of scramjet engines since the thickness of the boundary layer in the isolator/combustor plays an important role in the unstart process.[23,24] The mechanism by which the DBD actuator thins the boundary layer is likely related to the generation of spanwise flow,[11] as illustrated by the tunnel cross section schematic shown in Fig. 4. However, while Rayleigh scattering images are useful in characterizing the boundary layer thickness, this visualization cannot directly confirm the presence of induced spanwise motion in the boundary layer, and future experiments are underway to discern the detailed boundary layer velocity field using particle image velocimetry.

Despite the thinning effect of the DBD actuator on the local boundary layer, the shock induced by the ramp seems not to be greatly affected by the DBD, most likely because

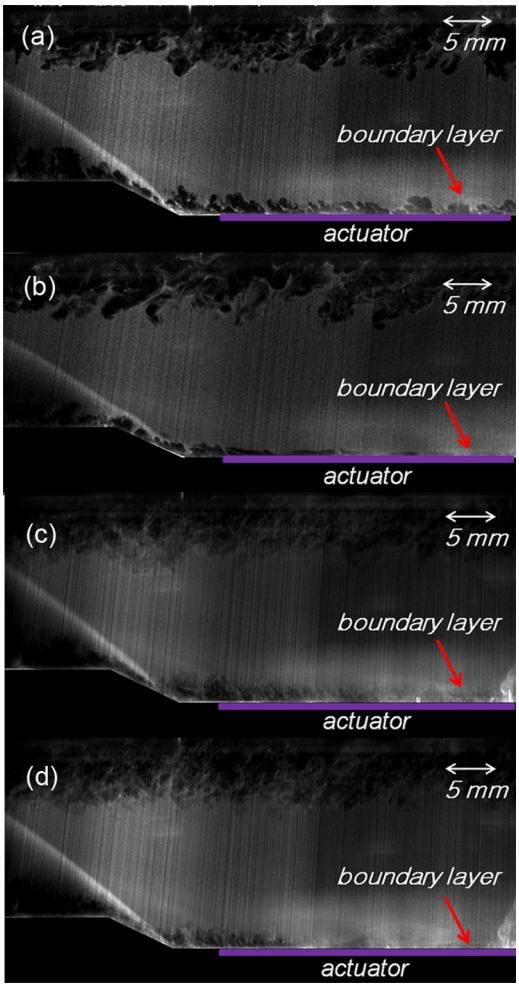

FIG. 3. (Color online) Instantaneous CO_2 Rayleigh scattering images (a) plasma off case, (b) plasma on case, averaged images, (c) plasma off case, and (d) plasma on case.

the actuation is highly localized, with the force generated near the centerline of the tunnel. The shock generated by the compression ramp spans across the tunnel, and is likely to be strongly influenced by the entire spanwise flow. Also, we see that the turbulent boundary layer appears to recover quickly in the region between the end of the actuator and the beginning of the compression ramp, further diminishing the propensity for actuation to affect the shock dynamics. Experiments are currently underway to extend actuation to the entire spanwise direction and to bring the actuation closer to the ramp.

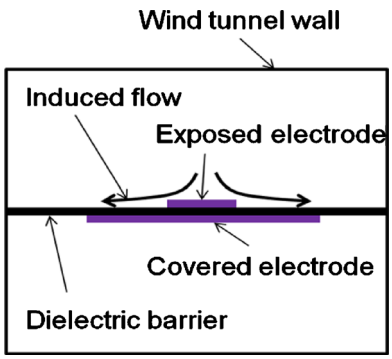

FIG. 4. (Color online) Schematic of spanwise motion induced be the DBD actuator.

In this paper, we demonstrate that the reduction in the turbulent boundary layer in supersonic flow is readily visualized by planar Rayleigh scattering off of condensed CO_2 particles. This effect of the DBD plasma actuator can be a potential method for control of turbulent boundary layer thickness in supersonic flow, which can lead to prevent or delay the inlet unstart of scramjet engine.

This work is sponsored by the Predictive Science Academic Alliance Program (PSAAP) at Stanford University, funded through the Department of Energy.

[1]E. Moreau, J. Phys. D **40**, 605 (2007).
[2]J. R. Roth, D. M. Sherman, and S. P. Wilkinson, Proceedings of the AIAA Meeting, Reno, Nevada, 1998.
[3]W. Kim, H. Do, M. G. Mungal, and M. A. Cappelli, Appl. Phys. Lett. **91**, 181501 (2007).
[4]H. Do, W. Kim, M. G. Mungal, and M. A. Cappelli, Appl. Phys. Lett. **92**, 071504 (2008).
[5]H. Do, W. Kim, M. G. Mungal, and M. A. Cappelli, Proceedings of the 45th AIAA Aerospace Science Meeting and Exhibit, Reno, Nevada, 2007.
[6]M. L. Post and T. C. Corke, AIAA J. **42**, 2177 (2004).
[7]J. Huang, T. C. Corke, and F. O. Thomas, AIAA J. **44**, 51 (2006).
[8]Y. Sung, W. Kim, M. G. Mungal, and M. A. Cappelli, Exp. Fluids **41**, 479 (2006).
[9]S. Grundmann and C. Tropea, Exp. Fluids **42**, 653 (2007).
[10]C. O. Porter, J. W. Baughn, T. E. McLaughlin, C. L. Enloe, and G. I. Font, AIAA J. **45**, 1562 (2007).
[11]D. M. Schatzman and F. O. Thomas, Proceedings of the 4th Flow Control Conference, Seattle, Washington, 2008.
[12]A. Santhanakrishnan and J. D. Jacob, J. Phys. D **40**, 637 (2007).
[13]N. Benard, J. Jolibois, G. Touchard, and E. Moreau, Proceedings of the 4th Flow Control Conference, Seattle, Washington, 2008.
[14]M. Kodera, S. Tomioka, T. Kanda, T. Mitani, and K. Kobayashi, Proceedings of the 12th AIAA International Space plane and Hypersonic Systems and Technologies Conference, Norfolk, Virginia, 2003.
[15]S. Leonov, V. Bityurin, N. Savischenko, A. Yuriev, and V. Gromov, Proceedings of the 39th AIAA Aerospace Sciences Meeting and Exhibit, Reno, Nevada, 2001.
[16]V. Narayanaswamy, L. L. Raja, and N. T. Clemens, AIAA J. **48**, 297 (2010).
[17]E. Menier, L. Leger, E. Depussay, V. Lago, and G. Artana, J. Phys. D **40**, 695 (2007).
[18]R. B. Miles, W. R. Lempert, and J. N. Forkey, Meas. Sci. Technol. **12**, R33 (2001).
[19]P. Wu, W. R. Lempert, and R. B. Miles, AIAA J. **38**, 672 (2000).
[20]T. C. Manley, Trans. Electrochem. Soc. **84**, 83 (1943).
[21]G. Nersisyan and W. G. Graham, Plasma Sources Sci. Technol. **13**, 582 (2004).
[22]J. Poggie, P. J. Erbland, A. J. Smits, and R. B. Miles, Exp. Fluids **37**, 438 (2004).
[23]G. Masuya, T. Komuro, and A. Murakami, J. Propul. Power **11**, 301 (1995).
[24]J. L. Wagner, K. B. Yuceil, A. Valdivia, N. T. Clemens, and D. S. Dolling, AIAA J. **47**, 1528 (2009).